Band gap narrowing in ferroelectric KNbO3-Bi(Yb,Me)O3 (Me=Fe or Mn) ceramics

PASCUAL-GONZALEZ, Cristina, SCHILEO, Giorgio and FETEIRA, Antonio

Published version

PASCUAL-GONZALEZ, Cristina, SCHILEO, Giorgio and FETEIRA, Antonio (2016). Band gap narrowing in ferroelectric KNbO3-Bi(Yb,Me)O3 (Me=Fe or Mn) ceramics. Applied Physics Letters, 109 (13).

Band gap narrowing in ferroelectric $KNbO_3$-$Bi(Yb,Me)O_3$ (Me=Fe or Mn) ceramics

Cristina Pascual-Gonzalez, Giorgio Schileo[#] and Antonio Feteira

Christian Doppler Laboratory for Advanced Ferroics, Materials Engineering and Research Institute, Sheffield Hallam University, Howard Street, Sheffield, S1 1WB, UK

#Now at Dyesol UK Ltd, UMIC, 48 Grafton Street, Manchester, M13 9XX, UK

Abstract

The direct optical band gap in ferroelectric $KNbO_3$-$Bi(Yb,Me)O_3$ (Me=Fe or Mn) ceramics fabricated by the solid state reaction method varies from 3.2 eV for $KNbO_3$ down to 2.2 eV for $0.95KNbO_3$-$0.05BiYbO_3$, as revealed by optical spectroscopic ellipsometry. This narrowing of band gap is accompanied by an apparent increase of the room-temperature relative permittivity from 320 for $KNbO_3$ to 900 for $0.95KNbO_3$-$0.05BiYbO_3$. All compositions studied exhibit dielectric anomalies associated with structural phase transitions and their ferroelectric nature is corroborated by the presence of a sharp mixed mode (at ~190 cm^{-1}) and by a Fano-type resonant dip in their Raman spectra.

Solar energy is one of the most promising sources of renewable, clean energy to replace our current dependence on fossil fuels. In conventional solid-state photovoltaics (for example Si-based solar cells), electron-hole pairs are created by light absorption and then separated using the potential developed at a p-n junction or heterojunction. The maximum photovoltage in these devices is equal to the semiconductor electronic band gap. In contrast, oxide ferroelectric (FE) perovskites (ABO_3) exhibit photovoltages exceeding several times their band gap values.[1] This abnormal photovoltaic effect in FE has been known for more than 50 years. Nevertheless, it has been largely disregarded for technological applications because in most oxide FE perovskites, the optical bands gaps are usually greater than 3 eV, limiting their light absorption primarily to the ultraviolet (UV) region, i.e. they are only able to capture ~ 8% of the solar spectrum. The wide optical band gaps in oxide FE perovskites arise from the nature of the bonding between O and B ions. Indeed, the large differences in electronegativity between the O and the B ions leads to the valence band to be formed by the 2p O states and the conduction band by the d states of the B transition metals sitting within the O octahedra. Until very recently, $BiFeO_3$ with a band gap of 2.7 eV was known to have the narrowest band gap among the oxide FE perovskites.[2] Nevertheless, $BiFeO_3$ is only able to capture 20% of the solar spectrum. $BiFeO_3$ thin films were observed to exhibit photovoltages that exceeded their band gap by several times.[3] The bulk nature of this phenomenon has been elegantly demonstrated by Bhatnagar et al.[4] A comprehensive study on how the crystal and defect chemistry influences band gap trends in alkaline earth perovskites was carried by Lee et al[5]. They found the optical band gap to vary systematically with tolerance factor and lattice volume within limits defined by the chemistry of the octahedral site.

Recently, Grinberg et al[6] demonstrated that the direct band gap of ferroelectric $(1-x)KNbO_3$-$xBaNi_{0.5}Nb_{0.5}O_{3-\delta}$ (KBNNO) ceramics can be tailor to values as low as 1.1 eV. Their first principle calculations have shown the valence band maximum to consist of hybridized Ni 3d

and O 2p states, while the conduction band minimum to be composed of Nb 4d states. Hence, they suggested that the filled Ni 3d gap states in KBNNO ceramics play a crucial part in narrowing the band gap. Band gaps of vacancy-free 75%$KNbO_3$-25%$(Pb_{0.5}Bi_{0.5})(Zn_{0.5}Nb_{0.5})O_3$ and 75%$KNbO_3$-25%$(Sr_{0.5}La_{0.5})(Zn_{0.5}Nb_{0.5})O_3$ were predicted from first principle calculations as 2.92 eV and 2.11 eV, respectively[7]. In this letter, we characterise the crystal structure, relative permittivity and band gap of $KNbO_3$ and self-compensated 95%$KNbO_3$-5%$BiYbO_3$, 95%$KNbO_3$-5%$BiFe_{0.5}Yb_{0.5}Fe_{0.5}O_3$ and 95%$KNbO_3$-5%$BiFe_{0.5}Yb_{0.5}Mn_{0.5}O_3$ ceramics. In relation to undoped $KNbO_3$ with a band gap of 3.2 eV, the narrower band gap among the three doped compositions is 2.2 eV and it is observed for 95%$KNbO_3$-5%$BiYbO_3$. This result shows that the presence of transition metals is not a necessary condition to lower the band gap. Moreover it also shows the need to further understand band gap engineering of ferroelectrics.

Dried K_2CO_3 (>99.0 %), Nb_2O_5 (>99.9 %, Aldrich), Bi_2O_3 (>99.9 %, Aldrich), Yb_2O_3 (>99.9 %, Aldrich), Fe_2O_3 (>99.0 %, Aldrich), and MnO_2 (>99.9 %, Aldrich) powders were weighed according to the $KNbO_3$ formula and self-compensated 95%$KNbO_3$-5%$BiYbO_3$, 95%$KNbO_3$-5%$BiFe_{0.5}Yb_{0.5}Fe_{0.5}O_3$ and 95%$KNbO_3$-5%$BiFe_{0.5}Yb_{0.5}Mn_{0.5}O_3$ formulae. These powders were placed into a 250 ml milling polyethylene bottle together with ~ 0.5 kg of yttrium-stabilized zirconia milling media and ~ 100 ml of propan-2-ol samples and then mixed on roller ball mill for ~20 hours. Mixed powders were dried and then passed through a 500 μm mesh sieve. The sieve powders were pressed into pellets and reacted between 500 and 1000 ^oC with intermittent re-grinding and re-firing until no change on X-ray diffraction (XRD) data was visible. The fully reacted powders were pressed as 8 mm pellets and fired up to 1070 ^oC for 2 hours. The pellets were stacked on top of each other and sintered in a closed alumina crucible to limit loss of K and Bi. Purity and crystal structure analyses were carried out by XRD using a Brucker diffractometer (model D8) set up in transmission geometry and using

monochromatic Cu $K\alpha_1$ radiation. XRD patterns were acquired in the 20 - 60 2θ range, with a step size of 0.02 degrees with a scan length of 2 seconds per step. Raman spectra were obtained with a Renishaw Raman microscope (model InVia) using a 532 nm solid state (100 mW) laser, in back-scattering geometry using a 50 cm^{-1} edge filter. Temperature dependent Raman measurements were carried out using a Linkam (THMS600) Temperature Controlled Stage. Modes were assigned according to literature data obtained from single crystals[8]. Platinum electrodes were coated onto the faces of the sintered pellets for electrical measurements. Capacitance measurements were carried out with a Solartron impedance analyser (model 1260) coupled with a computer-controlled furnace. Finally, samples were finely polished with colloidal silica for variable-angle spectroscopic ellipsometry measurements, which was carried out with a J. A.Woollam (model M2000) ellipsometer equipped with Glan–Taylor polarizers, a rotating compensator, deuterium and quartz halogen lamps for spectral coverage. Band gaps were estimated from the average of three measurements at 40º, 55º and 70º, and for each angle of incidence at least two measurements were taken. Data were fitted using a blank model with a Tauc-Lorentz oscillator. Direct optical band gaps were estimated by taking the zero-intercepts of the linear portion of the $(\alpha h\upsilon)^2$ vs hυ curves, where α and hυ are the absorption coefficient (in cm^{-1}) and the energy of the incident photon (in eV).[6]

Fig. 1 shows the room-temperature XRD data for $KNbO_3$ and self-compensated $95\%KNbO_3$-$5\%BiYbO_3$, $95\%KNbO_3$-$5\%BiFe_{0.5}Yb_{0.5}Fe_{0.5}O_3$ and $95\%KNbO_3$-$5\%BiFe_{0.5}Yb_{0.5}Mn_{0.5}O_3$ ceramics. Within the detection limits of the technique, undoped $KNbO_3$ ceramics appear to be single-phase and the symmetry of their crystal structure to be well described by the orthorhombic Amm2 space group. Residual $YbNbO_4$ (ICDD card # 00-023-1480) is detected in all doped compositions, as indicated by asterisks in Fig. 1(a). Lattice parameters for KN ceramics were calculated as a=3.9728(1) Å, b=5.6880(1) Å and c=5.7111(1) Å, which are in broad agreement with the ICDD card # 00-032-0822. XRD data for KN exhibits the typical

peak splitting expected for a perovskite with orthorhombic crystal symmetry, but within the resolution of our measurements only single peaks are visible for doped ceramics, as shown in Fig. 1(b). Nevertheless, those single peaks are asymmetric, indicating a clear lattice distortion away from perfect cubic symmetry. A closer inspection of the shoulders suggests the doped ceramics to still show an average orthorhombic crystal symmetry. This is further corroborated by the room-temperature Raman spectroscopy data in Fig. 2. Indeed, the typical spectral features exhibited by orthorhombic $KNbO_3$ are also visible in the Raman spectra of all doped ceramics. Basically, this spectral similarity is sufficient to describe all ceramics in the orthorhombic Amm2 space group, as explained later in more detail. Finally, XRD reflections for doped compositions shift towards lower 2θ angles, indicating an increase of the unit cell volume. It follows that $95\%KNbO_3$-$5\%BiYbO_3$ possesses the largest unit cell. This corroborates the Yb^{3+} B-site occupancy, as this cation has a larger ionic radius in comparison with Nb^{5+}, Fe^{3+} and Mn^{3+}. Comprehensive studies of the $KNbO_3$-$BiYbO_3$ and $KNbO_3$-$BiFe_{0.5}Yb_{0.5}Fe_{0.5}O_3$ systems will be presented elsewhere.

It can be anticipated that the simultaneous B-site occupancy by cations of very dissimilar ionic radius combined by the incorporation of Bi^{3+} in the A-site of the $KNbO_3$ lattice gives rise to local lattice distortions which cannot be discerned from the XRD data. For example, in a previous letter[9] we have shown the XRD data for $80\%KNbO_3$-$20\%BiYbO_3$ to be described by the cubic centrosymmetric $Pm\bar{3}m$ space group; however Raman spectroscopy revealed both the occurrence of local lattice distortions and the disruption of the long-range FE order. Hence, Raman spectroscopy analyses, Fig. 2, were employed to monitored changes to the local structure and to ascertain the FE nature of the materials, as described below.

From group theory analysis, the following 12 optical modes are expected for point group mm2: $4A_1 + 4B_1 + 3B_2 + A_2$. All these modes are Raman active, but since in our experiment the Raman spectra are unpolarized, modes of all symmetry species are collected the same time.

Hence, fewer modes are observed due to the overlapping and mixing of the modes. Assignment of modes in the Raman spectrum of $KNbO_3$ was carried out according to the single-crystal assignment by Shen et al[8]. Hence, in the low- to mid-wavenumber region the Raman spectrum of $KNbO_3$ is characterised by (i) a broad A_1 (TO) mode centered at 270 cm^{-1}, which is assigned to BO_6 bending, (ii) a Fano-type interference dip at 195 cm^{-1} and (iii) two sharp modes at 192 cm^{-1} and 296 cm^{-1}, respectively. Both (ii) and (iii) features are believed to be a fingerprint for the occurrence of long-range polar order in $KNbO_3$. The sharp mode at 192 cm^{-1} is actually a mixed mode due to B_1(TO), A_1(TO), A_1(LO) and B_2(TO) modes, whilst the mode at 296 cm^{-1} is due to A_1(LO) and A_1(TO), but because of the resolution limit of the instrument they appeared merged as a single peaks. The high wavenumber region (>500 cm^{-1}) of the Raman spectrum of $KNbO_3$ is characterized by a B_1(TO) mode (at ~ 532 cm^{-1}), a A_1(TO) modes (at ~596 cm^{-1}) and a A_1(LO) (at 834 cm^{-1}). Those are associated to vibrations of the octahedra. Upon doping new modes emerge, which here have been numerically labelled as 1 and 2, because at this stage information on their origin is merely speculative. The new mode 1 (~175 cm^{-1}) appears as a shoulder to the sharp mixed mode at 192 cm^{-1}. This mode is fairly stationary as it only shifts by ~ 2 cm^{-1} over the composition range $0 \leq x \leq 0.2$, as it will be shown elsewhere. In the past, this mode has been associated to A-O vibrations, in particular to nm-sized clusters rich in either Bi^{3+} or K^+ cations. Mode 2 appears around ~820 cm^{-1} and it has been previously associated with breathing of the octahedra, when occupied by different B cations.

In semiconductive FE materials, Raman spectroscopy analysis are more reliable to probe ferroelectricity than polarization, P, vs electric field, E, measurements. Indeed, often unsaturated PE loops can be observed for semiconductive non-FE materials. The two spectral features recognized as the fingerprint for long-range FE order in $KNbO_3$ are present in the Raman spectra of all doped compositions reported in this letter, as shown in Fig. 2.

Nevertheless, it is worth to mention that those two features are absent from the spectra of (1-x)$KNbO_3$-x$BiYbO_3$ ceramics for x≥0.10, as it will be presented elsewhere. Hence, long-range polar order is absent in (1-x)$KNbO_3$-x$BiYbO_3$ ceramics for x≥0.10 Actually, we have previously shown that long-range polar order in $KNbO_3$ is replaced by short-range polar order in (1-x)$KNbO_3$-x$BiYbO_3$ ceramics for x=0.20 and 0.30.[9] Those two compositions exhibit a so-called weak relaxor behaviour[9], which can be more specifically regarded as a re-entrant dipole glass behaviour[10].

The temperature dependence of the relative permittivity for $KNbO_3$ and 95%$KNbO_3$-5%$BiYbO_3$, 95%$KNbO_3$-5%$BiFe_{0.5}Yb_{0.5}Fe_{0.5}O_3$ and 95%$KNbO_3$-5%$BiFe_{0.5}Yb_{0.5}Mn_{0.5}O_3$ ceramics measured at 100 kHz is illustrated in Fig. 3. $KNbO_3$ shows two clear dielectric anomalies at 398 ^oC and 223 ^oC, which can ascribed to the cubic-to-tetragonal and to the tetragonal-to-orthorhombic structural phase transitions. On the single-crystal, these transitions were reported to occur on heating at 420 ^oC and 220 ^oC, respectively.[11] This may difference may be caused by the impurities present in the starting raw materials, in particular in K_2CO_3, which has the lowest purity. In 95%$KNbO_3$-5%$BiYbO_3$ ceramics, the tetragonal to cubic transition occurs at 353 ^oC, however the maximum permittivity occurs at 231 ^oC. This composition shows the highest relative permittivity over the entire temperature range considered. 95%$KNbO_3$-5%$BiFe_{0.5}Yb_{0.5}Fe_{0.5}O_3$ and 95%$KNbO_3$-5%$BiFe_{0.5}Yb_{0.5}Mn_{0.5}O_3$ ceramics show similar behaviour, the only difference is the apparent larger permittivity of the Fe-based ceramics.

In order to further evaluate the evolution of structural phase transitions and to assert the presence of long-range polar order, in-situ Raman spectroscopy analyses were carried out in the -180 to 280 °C temperature range. In Fig. 4, for the sake of simplicity, data is only presented for three different temperatures (-180°C, 120°C and 270°C), which are representative of the three ferroelectric polymorphic structures exhibited by $KNbO_3$. In Fig. 4(a), the spectra

collected at 270°C are consistent with the ferroelectric tetragonal polymorph. On cooling, the clear separation of the B_1(TO) and A_1(TO) modes in the 500-650 cm^{-1} region is consistent with the ferroelectric orthorhombic polymorph, as shown in Fig. 4(b) for data collected at 120°C. Finally, at -180°C, spectra in the 150-300 cm^{-1} region shows the spectral signature typical for the ferroelectric rhombohedral polymorph. It is worth the note that the aforementioned modes 1 and 2 are present at all temperatures. Hence, based on both permittivity measurements and Raman spectroscopy analysis all ceramics studied exhibit dielectric anomalies associated with structural phase transitions and their ferroelectric nature is corroborated by the presence of a sharp mixed mode (at ~290 cm^{-1}) and by a Fano-type resonant dip in their Raman spectra. Basically, all studied ceramics are ferroelectric in a wide temperature range.

Finally, the compositional dependence of the band gap values for $KNbO_3$ and self-compensated 95%$KNbO_3$-5%$BiYbO_3$, 95%$KNbO_3$-5%$BiFe_{0.5}Yb_{0.5}Fe_{0.5}O_3$ and 95%$KNbO_3$-5%$BiFe_{0.5}Yb_{0.5}Mn_{0.5}O_3$ ceramics is listed in Table I. These values were extrapolated from the Tauc's plot illustrated in Fig. 5. The value of the direct band gap for $KNbO_3$ is ~3.2 eV. This is very close to values reported elsewhere.[12] The narrowest direct band gap for the three doped compositions is 2.2 eV and is observed for 95%$KNbO_3$-5%$BiYbO_3$. This shows that the presence of transition metals is not a necessary condition to narrow the band gap of $KNbO_3$. The general broadening of the Raman modes from the doped ceramics, Fig. 4, results from increased lattice disorder, which manifests itself by the emergence of Urbach tails in the Tauc plots, Fig. 5.

It is also worth to mention that the apparent increase of the relative permittivity, Fig. 3, appears to follow the narrowing of the band gaps, Fig. 5. A correlation between the dielectric response and optical behavior of several other $KNbO_3$-based solid solutions, will be reported elsewhere.

Narrower band gaps (as low as 1.1 eV) are achievable for (1-x)$KNbO_3$-x$BaNi_{0.5}Nb_{0.5}O_{3-\delta}$ (KBNNO) ceramics[6], however oxygen vacancies may play a significant role on both the conduction and valence band energies, as postulated by Qi et al[13], in some cases it may narrow the band gap by ~ 0.5 eV. Unfortunately, the presence of oxygen vacancies is detrimental not only to polarization switching but can also trap the photogenerated carriers and increase the charge recombination rate as discussed by Wang et al[7], who used first principle calculations to estimate the band gaps for vacancy-free $KNbO_3$ co-doped with Zn and two different A-sites (A_1^{2+}=Pb^{2+}, Ba^{2+}, Sr^{2+} and A_2^{3+}=La^{3+}, Bi^{3+}) in order to achieve charge neutrality. The predicted bands gaps for those systems range between 2.92 eV to 2.11 eV. We our study, the experimental values of the optical band gaps for self-compensated doped $KNbO_3$ lie broadly within this range as shown in Fig. 5 and Table I. The minute amount of $YNbO_4$ is unlike to have any measurable impact on the dielectric properties and on band gap narrowing.

In summary, it was demonstrated that the band gap of $KNbO_3$ can be narrowed by 1 eV (i.e. a ~30% reduction) using dopants other than transition metals. Remarkably, band gap narrowing was achieved while maintaining long-range polar order over a wide temperature range.

Acknowledgments

The XRD and the Raman Microscope used in this research were obtained through the Birmingham Science City: Creating and Characterizing Next Generation Advanced Materials (West Midlands Centre for Advanced Materials Project 1), with support Advantage West Midlands and part funded by the European Regional Development Fund. Mr. L. Luisman is acknowledged for sample preparation and the performance of some measurements and Prof. A. Nabok for sharing its expertise on ellipsometry. This work was partially supported by Christian Doppler Research Association in collaboration with EPCOS OHG (a TDK group company).

References

[1] CS Tu, CM Hung, VH Schmidt, RR Chien, MD Jiang, and J Anthoninappen, Journal of Physics-Condensed Matter **24** (49) (2012).

[2] CM Hung, CS Tu, WD Yen, LS Jou, MD Jiang, and VH Schmidt, Journal of Applied Physics **111** (7) (2012).

[3] RK Katiyar, Y Sharma, P Misra, VS Puli, S Sahoo, A Kumar, JF Scott, G Morell, BR Weiner, and RS Katiyar, Applied Physics Letters **105** (17) (2014).

[4] A Bhatnagar, AR Chaudhuri, YH Kim, D Hesse, and M Alexe, Nature Communications **4** (2013).

[5] S Lee, WH Woodford, and CA Randall, Applied Physics Letters **92** (20) (2008).

[6] I Grinberg, DV West, M Torres, GY Gou, DM Stein, LY Wu, GN Chen, EM Gallo, AR Akbashev, PK Davies, JE Spanier, and AM Rappe, Nature **503** (7477), 509 (2013).

[7] FG Wang, I Grinberg, and AM Rappe, Physical Review B **89** (23) (2014).

[8] ZX Shen, ZP Hu, TC Chomg, CY Beh, SH Tang, and MH Kuok, Physical Review B **52** (6), 3976 (1995).

[9] L Luisman, A Feteira, and K Reichmann, Applied Physics Letters **99** (19) (2011).

[10] V Krayzman, I Levin, JC Woicik, and F Bridges, Applied Physics Letters **107** (19) (2015).

[11] G. Shirane, H. Danner, A. Pavlovic, and R. Pepinsky, Physical Review **93** (4), 672 (1954).

[12] WL Zhou, HM Deng, PX Yang, and JH Chu, Applied Physics Letters **105** (11) (2014).

[13] TT Qi, MT Curnan, S Kim, JW Bennett, I Grinberg, and AM Rappe, Physical Review B **84** (24) (2011).

Table I. Direct Optical Band Gaps.

Composition	Direct E_{gap} (eV)
$KNbO_3$	3.2
$95\%KNbO_3$-$5\%BiYbO_3$	2.2
$95\%KNbO_3$-$5\%BiFe_{0.5}Yb_{0.5}Fe_{0.5}O_3$	2.4
$KNbO_3$-$5\%BiFe_{0.5}Yb_{0.5}Mn_{0.5}O_3$	2.6

List of Figures

Fig. 1 Room-temperature XRD data in the (a) 20 to 60 (2θ) and (b) 44 to 58 (2θ) for $KNbO_3$, 95%$KNbO_3$-5%$BiYbO_3$, 95%$KNbO_3$-5%$BiFe_{0.5}Yb_{0.5}Fe_{0.5}O_3$ and 95%$KNbO_3$-5%$BiFe_{0.5}Yb_{0.5}Mn_{0.5}O_3$. (From bottom to top). Asterisk indicates residual $YbNbO_4$.

Fig. 2 Room-temperature Raman data for $KNbO_3$, 95%$KNbO_3$-5%$BiYbO_3$, 95%$KNbO_3$-5%$BiFe_{0.5}Yb_{0.5}Fe_{0.5}O_3$ and 95%$KNbO_3$-5%$BiFe_{0.5}Yb_{0.5}Mn_{0.5}O_3$. (From bottom to top)

Fig. 3 Temperature dependence of the relative permittivity of $KNbO_3$, 95%$KNbO_3$-5%$BiFe_{0.5}Yb_{0.5}Mn_{0.5}O_3$, 95%$KNbO_3$-5%$BiFe_{0.5}Yb_{0.5}Fe_{0.5}O_3$ and 95%$KNbO_3$-5%$BiYbO_3$. (From bottom to top)

Fig. 4 Raman spectroscopy data at (a) 270 °C, (b) 120 °C and -180 °C for $KNbO_3$, 95%$KNbO_3$-5%$BiYbO_3$ and 95%$KNbO_3$-5%$BiFe_{0.5}Yb_{0.5}Fe_{0.5}O_3$. (From bottom to top)

Fig. 5 Tauc plot for $KNbO_3$, 95%$KNbO_3$-5%$BiFe_{0.5}Yb_{0.5}Mn_{0.5}O_3$, 95%$KNbO_3$-5%$BiFe_{0.5}Yb_{0.5}Fe_{0.5}O_3$ and 95%$KNbO_3$-5%$BiYbO_3$. (From right to left)

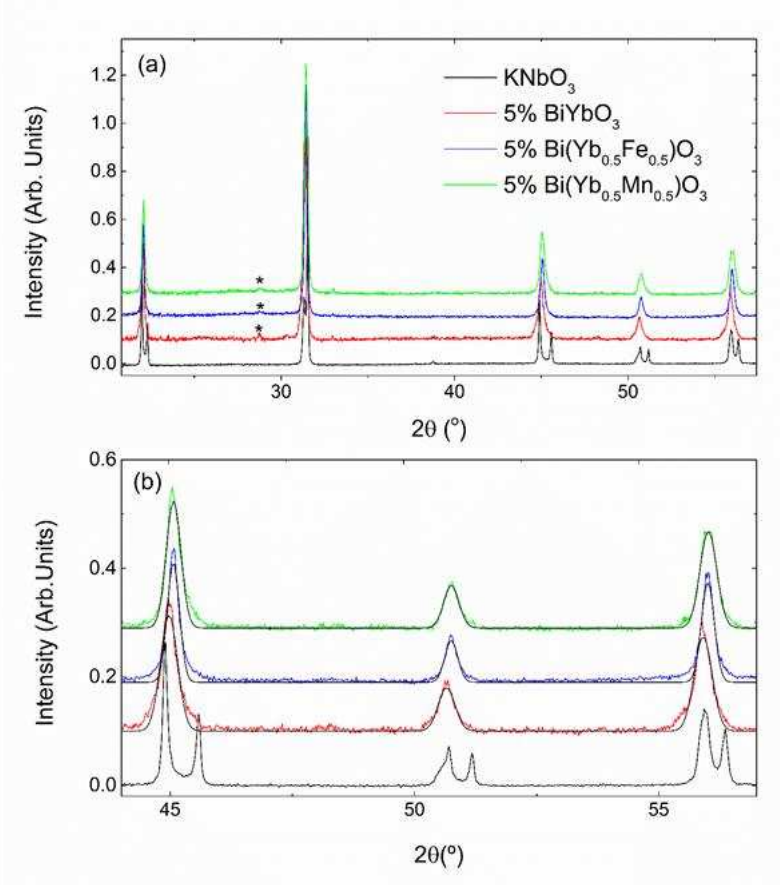

Fig. 1 Room-temperature XRD data in the (a) 20 to 60 (2θ) and (b) 44 to 58 (2θ) for $KNbO_3$, 95%$KNbO_3$-5%$BiYbO_3$, 95%$KNbO_3$-5%$BiFe_{0.5}Yb_{0.5}Fe_{0.5}O_3$ and 95%$KNbO_3$-5%$BiFe_{0.5}Yb_{0.5}Mn_{0.5}O_3$. (From bottom to top). Asterisk indicates residual $YbNbO_4$.

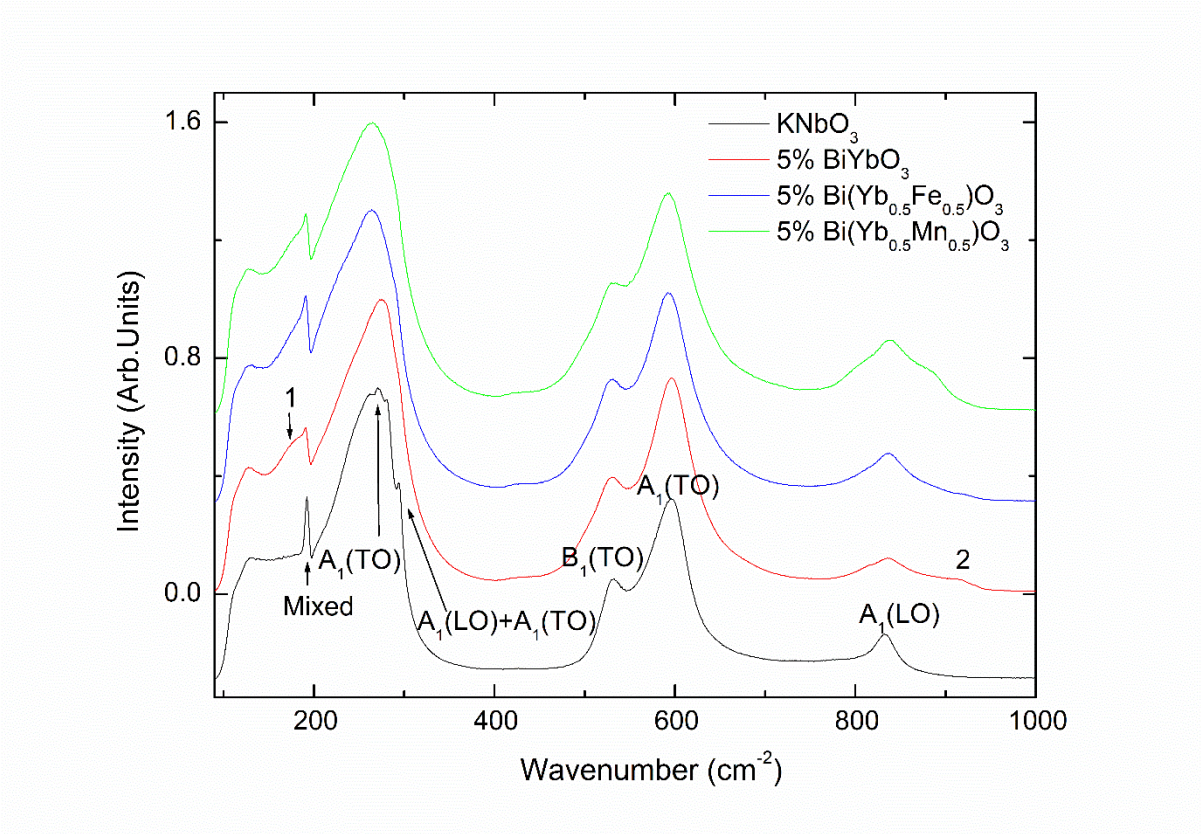

Fig. 2 Room-temperature Raman data for $KNbO_3$, 95%$KNbO_3$-5%$BiYbO_3$, 95%$KNbO_3$-5%$BiFe_{0.5}Yb_{0.5}Fe_{0.5}O_3$ and 95%$KNbO_3$-5%$BiFe_{0.5}Yb_{0.5}Mn_{0.5}O_3$. (From bottom to top)

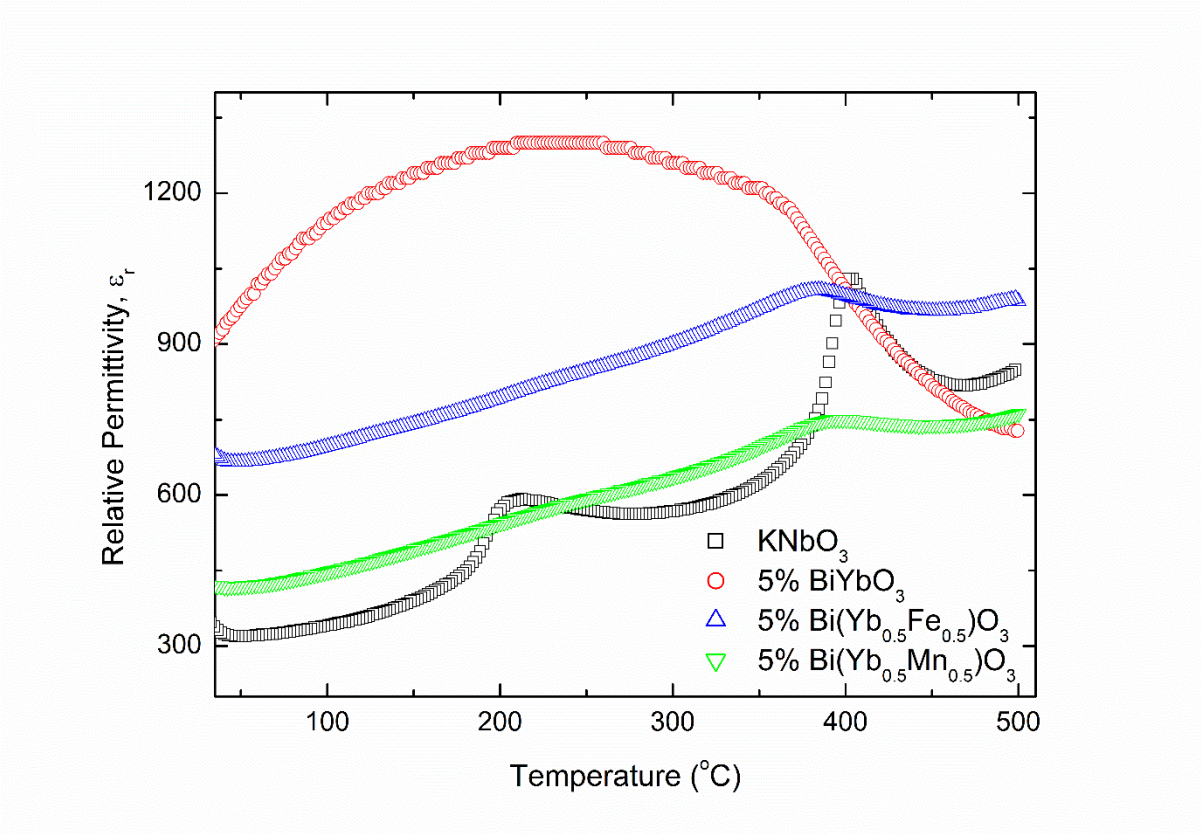

Fig. 3 Temperature dependence of the relative permittivity of $KNbO_3$, 95%$KNbO_3$-5%$BiFe_{0.5}Yb_{0.5}Mn_{0.5}O_3$, 95%$KNbO_3$-5%$BiFe_{0.5}Yb_{0.5}Fe_{0.5}O_3$ and 95%$KNbO_3$-5%$BiYbO_3$. (From bottom to top)

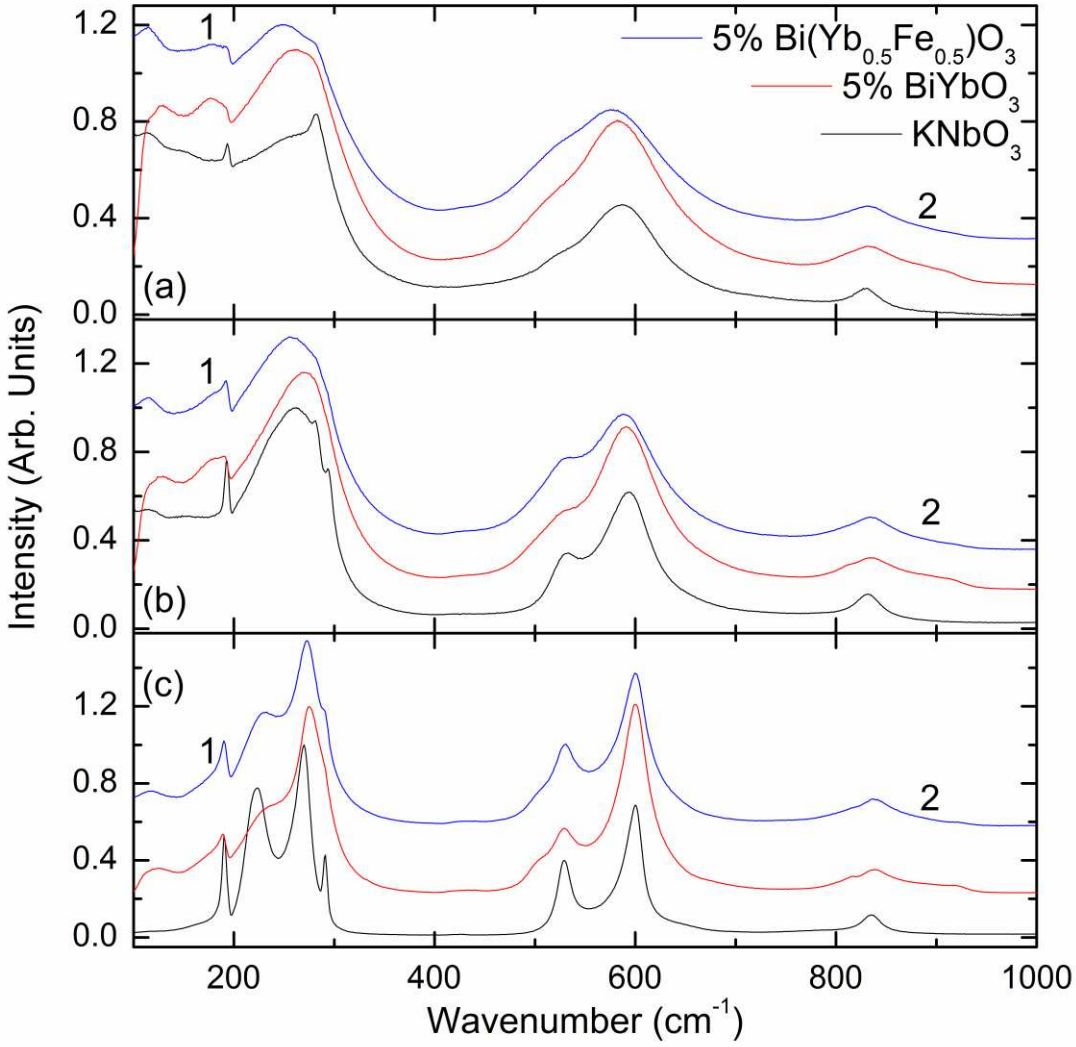

Fig. 4 Raman spectroscopy data at (a) 270 °C, (b) 120 °C and -180 °C for $KNbO_3$, 95%$KNbO_3$-5%$BiYbO_3$ and 95%$KNbO_3$-5%$BiFe_{0.5}Yb_{0.5}Fe_{0.5}O_3$. (From bottom to top)

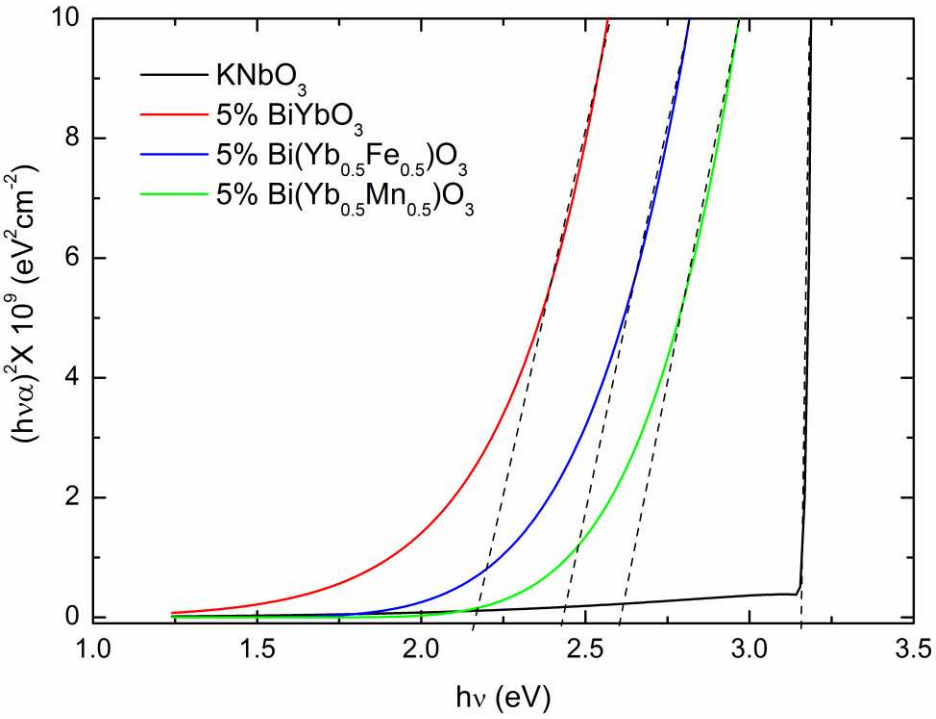

Fig. 5 Tauc plot for $KNbO_3$, 95%$KNbO_3$-5%$BiFe_{0.5}Yb_{0.5}Mn_{0.5}O_3$, 95%$KNbO_3$-5%$BiFe_{0.5}Yb_{0.5}Fe_{0.5}O_3$ and 95%$KNbO_3$-5%$BiYbO_3$. (From right to left)